ELSEVIER

Polymer 41 (2000) 8781–8789

polymer

www.elsevier.nl/locate/polymer

Transient rotator phase induced nucleation in *n*-alkane melts

E.B. Sirota*, A.B. Herhold

Exxon Mobil Research and Engineering Company, Corporate Strategic Research, Route 22 East, Annandale, NJ 08801, USA

In memory of Professor Andrew Keller

Received 4 October 1999; received in revised form 27 January 2000; accepted 4 February 2000

Abstract

A transient metastable rotator phase occurs on crystallization of *n*-alkanes into their triclinic crystalline phase from the supercooled melt. This was directly observed using time resolved X-ray scattering. The observed crystallization temperature is shown to be determined by the thermodynamic stability of the transient phase with respect to the liquid. The crystallization kinetics of the homologous series of *n*-alkanes was measured and explained in terms of a crossover from stability to "long-lived" metastability to transient metastability. This work highlights the importance of transient metastable phases in crystallization. © 2000 Elsevier Science Ltd. All rights reserved.

Keywords: Alkane; Nucleation; Rotator

1. Introduction

Many materials crystallize into metastable forms when cooling from the melt. This subject, as pertaining to polymers, has been recently reviewed by Keller and Cheng [1]. A metastable phase, once formed, may persist indefinitely, even far below its equilibrium transition temperature. Nucleation from the melt could also occur into a transient phase that converts to the stable form during some stage of growth. In such a case, there may be no temperature at which the metastable phase will remain indefinitely. Due to their ephemeral nature, transient phases are intrinsically difficult to observe and hence have been the subject of limited study. Transient phases are not only intermediate forms on the path to the final state [2] but can be key to understanding the process of crystallization. For example, the temperature at which the transient state can nucleate may determine the apparent temperature of crystallization for the stable phase. Polyethylene at high pressure is known to exhibit an equilibrium hexagonal phase between its low-temperature orthorhombic form and the liquid [3]. Keller and collaborators have extensively discussed the importance of the metastable extension of the hexagonal phase and its potential importance in polymer crystallization [1,4–12]. In addition, the properties of the metastable phase can determine the growth morphology of the crystal. For example, enhanced chain mobility in the metastable hexagonal phase may cause lamellar thickening in polyethylene [5].

The *n*-alkanes (C_nH_{2n+2}, abbreviated C_n) are interesting in their own right because of their rich behaviors. They are also the principle component of petroleum waxes and the building block of many derivative molecules whose properties are strongly influenced by their alkyl component [13–15]. In particular, polyethylene is the large-*n* limit of the alkanes. Ungar [14] has addressed this connection and the relation between the high-pressure hexagonal phase of polyethylene and the rotator phases of the shorter alkanes. The supercooling is the difference between the equilibrium transition temperature and the temperature where the transition actually occurs, on cooling. Recently, Kraack et al. [16] have shown that for homogenous nucleation (using the droplet technique), the crossover from the low characteristic supercooling behavior (~12°C) of *n*-alkanes ("wax") [17–20] to the large characteristic supercooling (~60°C) of polyethylene [21,22] occurs at relatively low chain-lengths ($n \sim 30$). It is thus clear that insight into the crystallization mechanisms of the shorter *n*-alkanes may have implications for higher-MW polymers.

Some of the most important information required to understand crystallization are the equilibrium thermodynamics and crystal structures. The crystallization kinetics and the supercooling exhibited by the system are of equal importance in understanding the macroscopic morphology of the crystals. On heating, solid–liquid transitions usually occur at their equilibrium temperature, thus "superheating" is rare. The *n*-alkanes exhibit a well-known even–odd effect

* Corresponding author.
E-mail address: ebsirot@erenj.com (E.B. Sirota).

PII: S0032-3861(00)00221-4

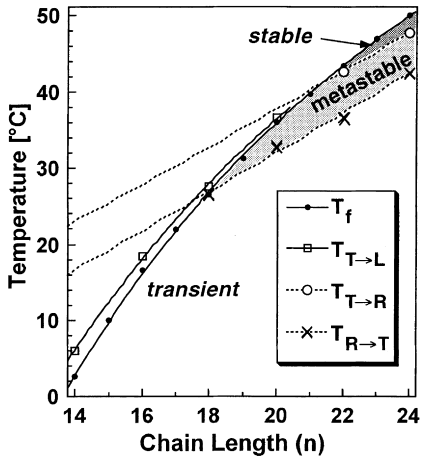

Fig. 1. Phase diagram of the *n*-alkanes. The dots are the freezing temperature T_f. The open squares are the melting temperature ($T_{T\to L}$) for those *n* which melt from the triclinic phase (*n*-even ≤ 20). The melting temperatures for the other *n* coincide with their freezing temperatures. The open circles are the triclinic-rotator phase transformation temperatures on heating ($T_{T\to R}$) and the crosses are the average rotator-triclinic transition temperatures ($T_{R\to T}$) on cooling at 0.07°C/min. The dashed lines are lines $T_{R\to T} = 37.71 + 2.47(n - 20)$ and $T_{T\to R} = 31.96 + 2.60(n - 20)$ and the solid curves are fits to the empirical form [61] yielding $T_f = 131.0(n - 13.66)/(n + 3.15)$ and $T_{T\to L} = 134.7(n - 13.13)/(n + 5.39)$. The regions labeled "stable," "metastable," and "transient" refer to the stability of the rotator phase for *n*-even.

in their melting points and crystal structures [13,23,24]. The kinetics and hysteresis, however, have remained a mystery. Using chain-length in the homologous series to tune the stability of the transient phase we have been able to: (i) provide a clear example of transient phase induced nucleation by direct observation and (ii) explain the kinetic behavior of *n*-alkane crystallization in terms of a crossover from "long-lived" to transient metastability [25].

Short *n*-alkanes exhibit various equilibrium rotator phases below their melting point and above their low-temperature crystal phase [14,15,26–33]. The rotator phases are lamellar crystals which lack long-range order in the rotational degree of freedom of the molecules about their long axes. In the equilibrium phase diagram for *n*-even, the rotator (R) phases are squeezed out at lower *n* by a triclinic (T) non-rotator crystal phase. Bulk melts of the *n*-odd alkanes ($15 \leq n \leq 29$) exhibit a liquid-rotator ($L \rightarrow R$) transition with negligible hysterisis [23,24,33]. The negligible supercooling of such bulk *n*-alkanes has been argued [24,34] to be related to the presence of an equilibrium surface monolayer rotator phase which is observed [35–41] at the liquid–vapor interface a few degrees above the crystallization temperature. This monolayer could serve as an ideal nucleation site for the bulk rotator phase. Ubiquitous tiny bubbles (in addition to the air–liquid surface) present in most bulk situations could thus act as such heterogeneous nucleation sites. The significant even–odd effect in the equilibrium melting points (for $n < 22$) can be associated with whether melting is from the triclinic crystal (*n*-even ≤ 20) or from the rotator phase (*n*-odd and *n*-even ≥ 22) [23,24]. However, the even–odd effect disappears when considering the observed freezing temperatures (Fig. 1) because the *n*-even which have high melting points supercool, whereas the *n*-odd, which crystallize into the rotator phase, do not. Is it a coincidence that the amount of supercooling for *n*-even ($n \leq 20$) is equal and opposite to the even–odd difference in the melting temperatures? [24]. No. We have demonstrated experimentally that short *n*-even alkane chains crystallize via a transient rotator phase [25].

The paper is organized as follows. We will first describe the details of the direct observation of the transient rotator phase in C_{16} using high brightness synchrotron X-rays, and then the observation of the transient rotator phase in C_{18} using a rotating anode X-ray source. Next we present details of the measurements of the transition temperatures and the resulting chain-length dependent kinetic phase diagram for C_{13}–C_{25}. Finally, we end with general discussion and conclusions.

2. Experiment and results

2.1. C_{16} kinetics

We studied the time-dependent X-ray scattering of C_{16}, which unambiguously exhibits a supercooling of ~1.5°C on crystallizing from the melt and is energetically far away from exhibiting a stable bulk rotator phase [25]. In contrast, C_{22} shows a stable rotator phase on both heating and cooling, and C_{20}, only on cooling. Experiments were performed at the National Synchrotron Light Source on Exxon's beamline X10A using 8 keV radiation and a Braun position-sensitive 1D detector (PSD). The PSD was located 70 cm from the sample and had an active length of 5 cm and width of 1 cm. A small quantity (~0.8 mg) of C_{16} (Aldrich, >99% anhydrous) was placed at the bottom of a quartz capillary which was contained in a temperature controlled copper cell. The sample was small enough to be entirely illuminated by the 1.5 mm (hor.) × 1 mm (vert.) beam.

The stable crystalline form of C_{16} is the triclinic crystal phase in which the molecules are tilted with respect to the layers by 19.4° [42]. The 001 reflection at $q = 2\pi/d = 0.305$ Å^{-1} corresponds to a layer spacing of $d = 20.6$ Å. The in-plane packing of this phase gives rise to principle reflections at $q = 1.374$, 1.658, and 1.753 Å^{-1}, as well as mixed reflections. The PSD was centered at $q = 0.29$ Å^{-1} ($2\theta = 4°$) to detect the 001 lamellar reflection, or at $q = 1.58$ Å^{-1} ($2\theta = 22°$) to probe the higher-q in-plane reflections.

Due to the stochastic nature of nucleation and the fact that any single crystallite could only be observed if it were oriented at a correct angle with respect to the detector, we automated the cooling process and recorded 85 cycles. We heated the sample ~10°C above the melting temperature, T_m, and then cooled to just below the temperature at which

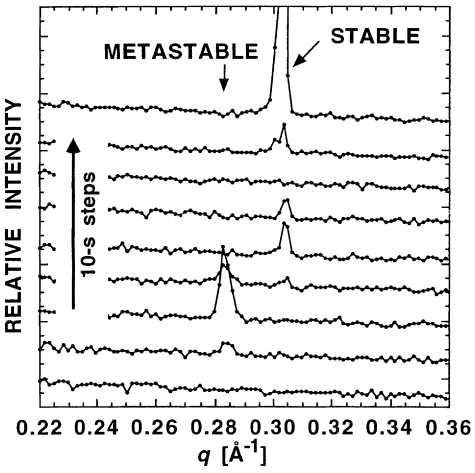

Fig. 2. Intensity versus q as a function of time showing the 001 lamellar peak of C_{16} during crystallization. The metastable peak develops at $q = 0.286$ Å^{-1} and the stable peak later appears $q = 0.305$ Å^{-1}. The scans were taken in 10 s steps and are offset vertically.

crystallization could be observed. Using a slow cooling rate of ~0.03°C/min, we observed the onset of the triclinic phase at 16.51°C. Averaged over 10 s intervals, we recorded data from the PSD while cooling at 0.5°C/min to a final temperature of 16.4°C. The first peaks appeared at the same time within each cycle (±15 s).

We obtained X-ray scattering peaks from a transient phase 9 times out of the 85 cooling cycles. In Fig. 2, we show the scattering at low angles as a function of time for one such case. A peak first develops at $q = 0.286$ Å^{-1} and then subsequently disappears as the peak at $q = 0.305$ Å^{-1} develops. (In these early stages of crystallization of a pure short *n*-alkane which may eventually form millimeter sized crystals, there are only a few crystallites formed which can rotate in the liquid and must be oriented fortuitously in order to be detected. The total peak intensity therefore cannot be used to quantitatively represent the total crystallized fraction, as it can in many polymer systems where a powder average can be assumed [43]). The peak from the transient phase was visible for ~20 s and its position suggests untilted molecules. Since $q = 0.305$ corresponds to a 19.4° tilt, we would expect and indeed observe a peak near $q \approx 0.305 \cos(19.4°) = 0.2875$ for zero tilt. Three other cooling cycles produced similar results in which the peak intensity of the transient phase at $q = 0.286$ Å^{-1} was weaker, but still unambiguous (comparable to the fourth curve in Fig. 2) and with lifetimes of ≤10 s. Four cycles yielded very weak peaks at $q = 0.286$ Å^{-1} lasting for ≤10 s. In one cycle, the transient phase remained for almost 8 min, and in Fig. 3 we show high-angle scans taken during that cooling run. The three plotted scans were taken at 30 s intervals. Prior to these scans, the lamellar peak was at $q = 0.286$ Å^{-1}, and after these scans, at $q = 0.305$ Å^{-1}. The diffraction pattern shown in Fig. 3(c) is that expected for the stable triclinic phase of C_{16}. The peak positions of the transient phase appeared at $q = 1.498$ Å^{-1} and $q = 1.632$ Å^{-1}. Fig. 3(b) shows coexistence of both the phases. The peak positions of the transient phase are distinct from any peaks exhibited by the stable triclinic crystal phase. Assignment of the transient peaks will be discussed together with the C_{18} data in the following section.

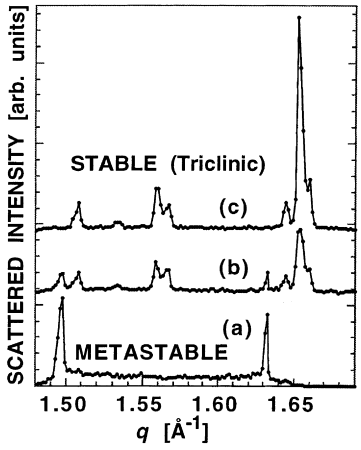

Fig. 3. Intensity versus q at 30 s intervals showing the in-plane peaks of C_{16} transforming from the transient metastable phase to the stable phase.

2.2. C_{18} kinetics

The crystallization of C_{18} was studied using time dependent X-ray scattering and was performed on a 18 kW Rigaku X-ray generator with a Huber goniometer. Cu K_α radiation was used and the beam was defined with a bent graphite monochromator and slits, giving a resolution of $\Delta q = 0.01$ Å^{-1}. A Bicron single channel detector was used. C_{18} (Aldrich, >99%) was contained in a 2 mm thick copper sample holder with Be windows in a temperature controlled oven. Temperature gradients in the oven lead to absolute uncertainties of <0.1°C.

The stable form of C_{18} is the triclinic crystal phase in which the molecules are tilted with respect to the layers by ~20° [42,44]. This phase supercools ~1°C when crystallizing from the melt. In Fig. 4(a) we show high angle scans corresponding to the in-plane packing of C_{18} in the stable triclinic crystal phase. Reflections are seen at $q = 1.366$, 1.399, 1.487, 1.569, and 1.650 Å^{-1}. Since we used a single channel detector rather than a PSD, data collection was slow. However, since the lifetime of the transient phase is stochastic, we were able to collect a full scan in that phase by repeating the experiment until a cooling run occurred with a lifetime long enough to measure the spectrum. As is seen below in the histograms of the lifetimes for C_{18} (Fig. 7), this was quite feasible. The primary peak positions in the metastable phase of C_{18} were $q = 1.496$ and 1.609 Å^{-1} (Fig. 4(b)). A peak at $q = 1.536$ Å^{-1} is a higher order mixed reflection which occurs in the R_I rotator phase.

The alkanes with *n*-odd ($n \leq 21$) exhibit an equilibrium orthorhombic rotator phase (R_I), where the molecules are untilted with respect to the layers [26–32]. To clarify the

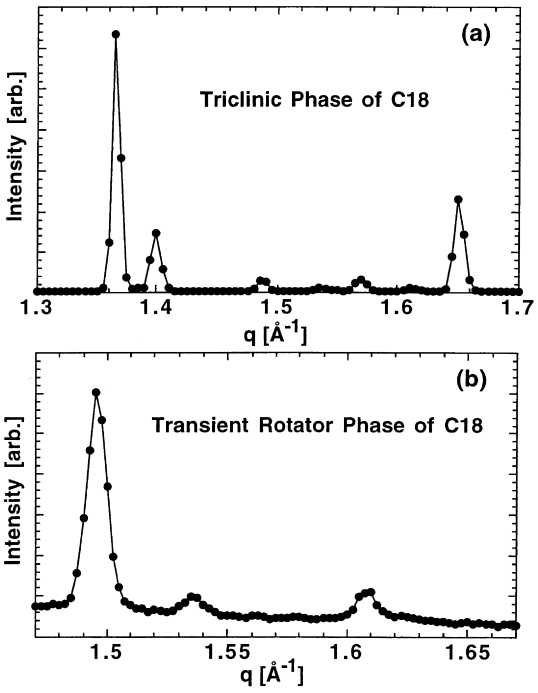

Fig. 4. Intensity versus q for C_{18}. (a) Triclinic phase. There is little diffuse scattering and peaks occur at well-defined positions $q = 1.366$, 1.399, 1.487, 1.569, and 1.650 $Å^{-1}$. (b) A q-scan caught in the transient rotator phase, showing peaks at $q = 1.496$, 1.536 and 1.609 $Å^{-1}$.

nature of the observed transient phase, we plot in Fig. 5 the peak positions of the R_I rotator phase just below the freezing temperature T_f for *n*-odd alkanes, along with the positions observed here for C_{18} and C_{16} [25]. It is clear from this data that the peak positions observed for the transient phase correspond to the interpolated peak positions expected for the rotator phase. Also depicted are the peak positions of the untilted, orthorhombic, non-rotator, herringbone crystal phase of the *n*-odd alkanes, which unambiguously differ from those of the transient phase.

To investigate the kinetics of the transient phase of C_{18}, we first performed "isothermal" experiments consisting of

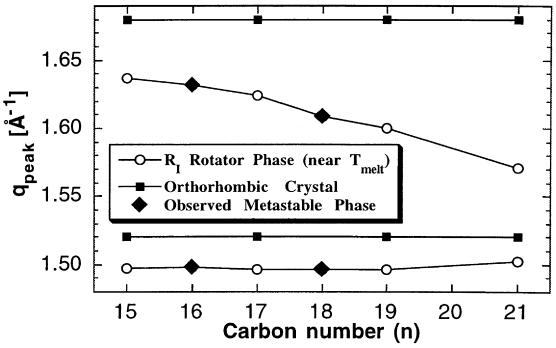

Fig. 5. The peak positions in the stable R_I rotator phase just below the melting temperature (circles) and in the low-temperature orthorhombic herringbone crystal phase (squares). The observed positions of the peaks in the metastable phase of C_{18} and C_{16} [25] (diamonds) are consistent with the rotator phase.

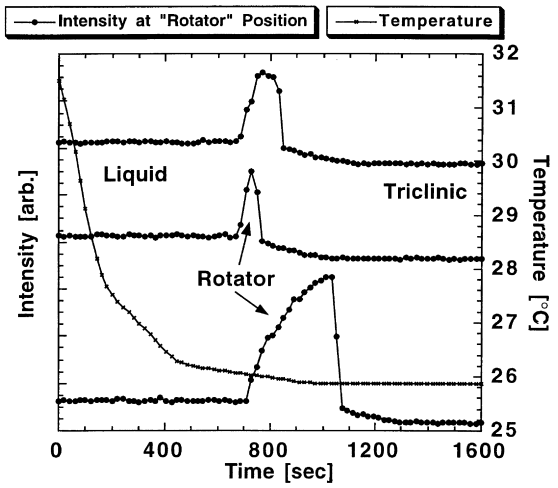

Fig. 6. Intensity sitting at $q = 1.496$ $Å^{-1}$ for three typical runs obtained at cooling C_{18} to 0.19°C below the highest observed crystallization temperature. At early times, the sample is in the liquid phase, and at long times the sample is in the triclinic crystal phase. The scattering level of the liquid phase is greater than that of the crystal phase. The high intensity at this q position is associated with the transient rotator phase, which exhibits a peak at that position. Also depicted is the temperature as a function of time for this series of runs.

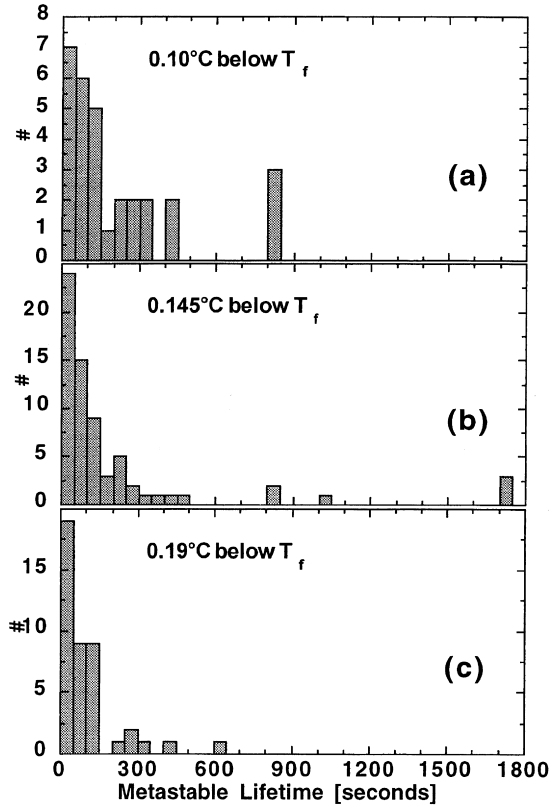

Fig. 7. Histograms of the lifetime of the metastable rotator phase in C_{18} when cooling at 0.056°C/min and sitting at (a) 0.10, (b) 0.145 and (c) 0.19°C below the temperature of the onset of crystallization. In (a) the values at 800 s imply (≥800 s) and in (b) the values at 1750 s imply ≥1750 as discussed in the text.

Table 1
Measured transition temperatures as described in the text (all in °C)

n	T_f	$T_{R\to L}$ end	$T_{R\to L}$ 50%	$T_{T\to L}$ 50%	$T_{T\to L}$ end	$T_{T\to L}$ seeded	$T_{R\to T}$	$T_{T\to R}$ 50%	$T_{T\to R}$ end	$T_{T\to R}$ seeded
13	− 5.56	− 5.06	− 5.18							
14	2.58			5.77	5.95	5.59				
15	10.05	10.38	10.25							
16	16.51			18.51	18.39	17.98				
17	21.89	22.14	21.93							
18	26.56			27.45	27.65	27.40	26.48			
19	31.19	31.46	31.15							
20	35.95	36.27	36.05	36.41	36.59	36.21	32.70			
21	39.75									
22	43.34	43.58	43.33				36.57	42.55	42.65	42.53
23	46.94	47.10	47.02							
24	49.89	50.11	49.93				42.49	47.39	47.59	47.17
25	53.03	53.23	53.05							

slow quenches to fixed temperatures. The sample was first entirely melted (>10°C above the melting temperature for at least 15 min) and then cooled through the freezing point at 0.056°C/min to a fixed temperature slightly below T_f. T_f is defined as the highest temperature where any crystallization was observed, as measured when cooling at 0.03°C/min. The scattering intensity was monitored at $q = 1.496$ Å^{-1}, a position corresponding to a peak in the R_I phase (and not a peak of the triclinic phase). This measurement was repeated many times for three different isothermal temperatures: $T_f - 0.10$°C, $T_f - 0.145$°C, and $T_f - 0.19$°C ($T_f = 26.56$°C for C_{18}).

In Fig. 6 we show results of three typical quench experiments, all at $T_f - 0.19$°C. The increase and decrease in intensity is associated with the appearance and subsequent disappearance of the rotator phase. The finite intensity present before the rotator phase appears is due to the broad liquid-peak centered at $q = 1.35$ Å^{-1}. Since there is little diffuse scattering in the final triclinic crystal phase, the intensity at $q = 1.496$ Å^{-1} drops below that of the liquid phase. The lifetime of the transient rotator phase can be unambiguously determined from such scans. Since the lifetime is stochastic, each run was different.

The observed lifetimes of the transient phase are shown as histograms in Fig. 7. For the $T_f - 0.10$°C quenches (Fig. 7(a)), the maximum observation time was 800 s from the appearance of the rotator phase. Therefore, the three points plotted at 800 s were actually lifetimes ≥800 s. Similarly, for the $T_f - 0.145$°C quenches (Fig. 7(b)), the three data points at 1750 s represent lifetimes ≥1750 s. For the $T_f - 0.19$°C quenches (Fig. 7(c)), 620 s was the longest lifetime observed and was less than the observation time (so the rotator phase always converted to the triclinic during the observation). Since some of the lifetimes were beyond the experimental observation time, and since the maximum observation time was not constant for all quench temperatures, we computed an "effective" average lifetime by counting all lifetimes >800 s as 800 s. For quenches to $T_f - 0.10$°C, $T_f - 0.145$°C, and $T_f - 0.19$°C we obtained average lifetimes of 209, 166, and 101 s using 30, 68, and 43 data points, respectively. (The true lifetimes for the first two were even longer due to the truncation of the long time data.) Another type of measurement, cooling continuously through the transition at ~0.07°C/min, gave a metastable lifetime of 97 s, averaged over 38 runs. We thus see that the lifetime of the metastable phase decreases with decreasing temperature.

2.3. Chain-length dependent phase diagram for C_{13}–C_{25}

The above results clearly show that for C_{16} and C_{18}, a transient rotator phase occurs upon crystallization from the supercooled melt. The distribution of transient phase lifetimes raises the issue of what determines the kinetics of conversion from the R phase into the stable triclinic phase. Systematic measurements of the chain-length dependence of the various transition temperatures on C_{13}–C_{25} were performed using X-ray scattering and are tabulated in Table 1. These transition temperatures are shown in Fig. 1 and are scaled to the freezing point in Fig. 8. The various transition temperatures are defined as follows: T_f

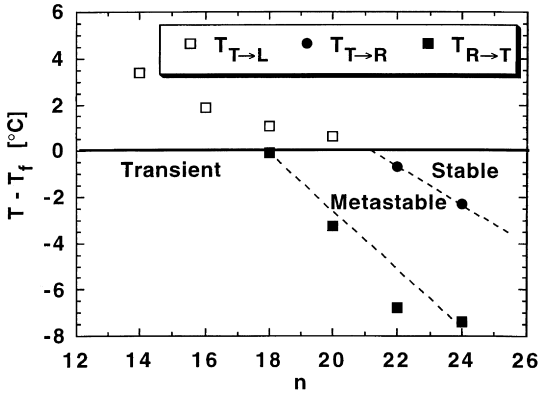

Fig. 8. The transition temperatures as in Fig. 1, but with temperature plotted with respect to T_f in order to enhance the features.

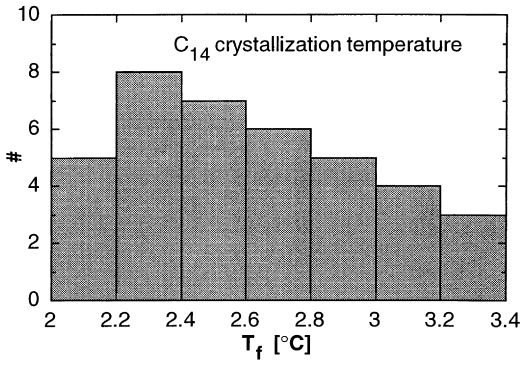

Fig. 9. Histogram of the observed crystallization temperature of C_{14} for multiple cooling runs with rates varying from 0.011 to 0.07°C/min.

denotes the temperature where crystallization is first observed (cooling slowly at 0.03°C/min). For the chain-lengths where the L ↔ R transition can be observed both on heating and cooling (i.e. even $n \geq 20$ and all odd-n), $T_{R\rightarrow L}$ and T_f agree within their uncertainty, consistent with the negligible supercooling reported for this transition [23,24,33]. The points labeled $T_{T\rightarrow L}$ are the temperatures at which the triclinic crystal melts to the liquid (even $n \leq 20$). $T_{T\rightarrow R}$ is the temperature where the triclinic phase transforms to the rotator phase on heating (even $n \geq 22$). Since adiabatic scanning calorimetry demonstrated that the T → R transition does not superheat [33], $T_{T\rightarrow R}$ can be considered the equilibrium temperature of the T ↔ R transition. $T_{R\rightarrow T}$ is the average temperature at which a rotator phase transforms to the triclinic phase when cooling at a rate of 0.07°C/min. In a sense, $T_{R\rightarrow T}$ can be considered the temperature below which the R → T transition is likely to occur on a "reasonable" time scale. $T_{R\rightarrow T}$ and $T_{T\rightarrow R}$ vs. n are virtually parallel, showing that the supercooling of the R ↔ T transition is ~6°C.

We now describe the experimental collection of the transition temperatures tabulated in Table 1 and shown in Figs. 1 and 8. The n-alkanes were >99% pure from Aldrich and used as obtained. The X-ray scattering apparatus, sample holder, and oven were the same as described above for C_{18}. Experiments were performed by monitoring the intensity at a peak position associated with either the initial or final phase.

Specifically, in the case of cooling from the melt, some experiments were performed by monitoring the intensity of the broad liquid peak at $q \sim 1.35$ Å^{-1} (where we were sure to avoid the position of the sharp triclinic crystal peak in that region, for the n-even alkanes). Crystallization was determined by the first point statistically lower than the intensity observed in the liquid phase. The temperatures determined by using the peaks of the high temperature phase and the low temperature phase gave equivalent results for all these transitions.

T_f: The temperature of the first onset of crystallization, T_f, was determined by performing 10–20 measurements at a constant cooling rate of 0.03°C/min and noting the *highest* temperature observed for the onset of crystallization. Measurements done as slowly as 0.007°C/min did not produce any higher reported temperatures. Thus, the cooling rate of 0.03°C/min was slow enough to give values for T_f which were independent of cooling-rate. While we report the *highest* observed temperature of crystallization from the melt, we note that the crystallization temperatures on multiple runs varied by only about 0.05°C, in contrast to the rotator-triclinic transition temperature described below. An exception was C_{14}, where T_f had a larger spread of ~1°C with an average value of 2.62°C and a maximum value of 3.26°C. This spread was calculated from a total of 38 runs with cooling rates varying from 0.011 to 0.07°C/min with no noticeable dependence on cooling rate. A histogram for this observed distribution in T_f for C_{14} is shown in Fig. 9.

$T_{R\rightarrow L}$: For n where the rotator phase was stable, we could also measure the melting point of this phase, $T_{R\rightarrow L}$. We tabulated both the temperature at which the intensity of the liquid peak reached its full value ("end-of-melting"), which puts an upper limit on the melting point, as well as the temperature where 50% of the intensity was recovered ("50% melted"). The smearing of melting by impurities is rather narrow (<0.1°C as determined previously by adiabatic scanning calorimetry [33]) and not of significance here. The $T_{R\rightarrow L}$ reported in Table 1 were collected at a heating rate of 0.0077°C/min. (We also performed melting curves at faster rates, up to 0.055°C/min). Extrapolating linearly to zero heating rate would result in a reduction of the reported "end of melting" and "50% melted" temperatures by ~0.07°C. The data, however, is presented as measured. In Fig. 10 we plot $T_{end\text{-}melt} - T_f$; for $n > 13$ this is approximately 0.25°C. After accounting for the possible steady-state temperature gradients across the cell and the extrapolation to zero cooling rate, these values are consistent with the negligible supercooling observed at the liquid-rotator transition in bulk [23,24,33]. For C_{13}, $T_{end\text{-}melt} - T_f$ is almost twice as large and may be due to more significant supercooling occurring due to the lack of surface crystallization in the shorter chain-lengths of n-alkanes ($n < 15$) [38].

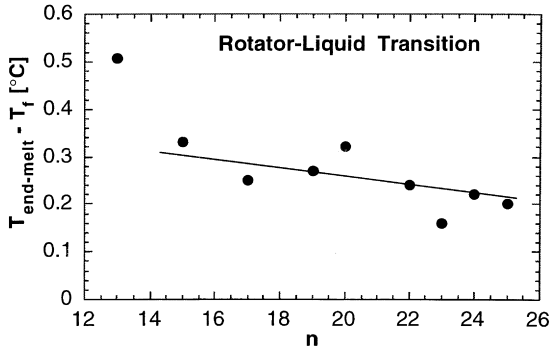

Fig. 10. $T_{end\text{-}melt} - T_f$ measured at 0.0077°C/min as a function of chain-length.

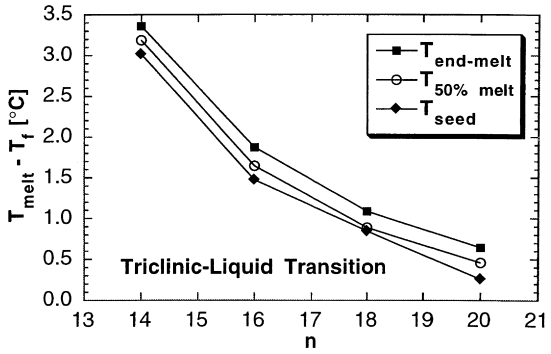

Fig. 11. Melting of the triclinic phase: the "end-of-melting" temperature, the "50%-melted" temperature, and the "seeded" crystallization temperature, all offset from T_f.

$T_{T\to L}$: To determine the equilibrium melting temperature of the triclinic phase for *n*-even $14 \le n \le 20$, we melted the sample at heating rates as low as 0.0077°C/min, and noted the "end-of-melting" as well as the "50% melted" temperatures. Again, extrapolating to zero cooling rate would reduce these values by only ~0.07°C.

We also performed a seeded-crystallization measurement to remove any nucleation barrier for crystallization. For this, we heated until ~50% was melted and then started cooling at 0.0077°C/min and noted the temperature at which the liquid scattering intensity began to decrease again. This allowed us to determine the temperature of crystallization from the liquid to the triclinic phase with triclinic seed crystals. With seed crystals, crystallization occurs at a higher temperature than the usual rotator-phase-mediated crystallization. This also allows us to bracket and establish error bars on the thermodynamic equilibrium temperature of the transition between the liquid and triclinic phase. In Fig. 11, we show the "end-of-melting" temperature, the "50%-melted" temperature, and the "seeded" crystallization temperature, all scaled to T_f. These all are within 0.4°C of each other and show the same trends with chain-length. The "end-of-melting" for $T_{T\to L}$ is plotted in Fig. 1.

$T_{T\to R}$: The R ↔ T transition exhibits substantial hysterisis. The temperature of the triclinic to rotator transition on heating, which was observed only for $n = 22$ and $n = 24$, was determined in a way similar to the triclinic to liquid transition. We determined the "end-of-melting", "50% transformed", and "seeded" crystallization temperatures (Fig. 12). Here we sat both at the position of the rotator phase peak and at the triclinic phase peak, obtaining consistent results. Since, as mentioned earlier, this transition does not superheat, these temperatures bracket the equilibrium temperature for the T ↔ R transition.

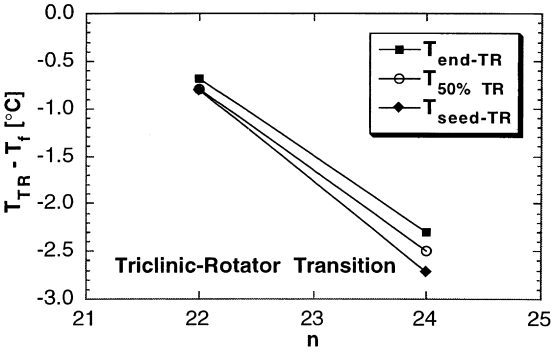

Fig. 12. T → R transition on heating: the "end-of-transformation" temperature, the "50%-transformed" temperature, and the "seeded" transformation temperature, all offset from T_f.

$T_{R\to T}$: The temperature of phase transition was measured by sitting at a peak position of the triclinic phase and cooling at 0.07°C/min. The reported values are for the average of 10–40 runs. For C_{18}, at this cooling rate, the average transition temperature $T_{R\to T}$ is below T_f, meaning that the rotator phase is almost always observed. However, the lifetime is always finite. This is in contrast to C_{20}, C_{22}, and C_{24}; for which a rotator phase can last indefinitely when sitting between T_f and $T_{R\to T}$. As can be seen in the histogram of the observed transition temperatures on cooling C_{20} (Fig. 13), the R → T transition is highly stochastic in nature giving a wide distribution of measured transition temperatures [45]. There is also noticeable cooling rate dependence to this transition, even for the slow rates used here. For example, cooling C_{22} at 0.02°C/min gives an average transition temperature of 37.69°C, while at 0.15°C/min the average transition temperature is 36.11°C.

3. Discussion and conclusions

We thus see that the chain-length-dependent phase diagram contains a crossover in the *n*-even alkanes from a stable rotator phase ($n \ge 24$) to a metastable rotator phase ($n = 20, 22$) to a transient rotator phase ($n \le 18$). For C_{18}, the rotator phase is on the border of transience and is rather long-lived (and hence observable using a rotating anode X-ray source). For C_{16}, it is observable only with time-dependent synchrotron scattering. For C_{14}, where T_f is 20°C below the extrapolated $T_{T\to R}$ line, one would not expect to directly observe the transient phase. However, it nevertheless controls T_f. In Fig. 14, we schematically show the relative free energies of the three phases for the stable, metastable and transient cases, and illustrate the path taken on cooling and heating. These diagrams show how the phase behavior varies, and can be related to a continuous shift of the rotator phase free energy.

We have shown that it is no coincidence that the fact that the temperature at which the supercooled liquid transforms to the triclinic phase (for *n*-even alkanes) lies on the same curve as where the rotator phase would be stable with respect to the liquid. Rather, it results from the fact that crystallization of the triclinic phase is mediated by a transient rotator phase. The recognition of the importance of such transient phase nucleation may help explain not only crystallization from the melt, but also crystallization from

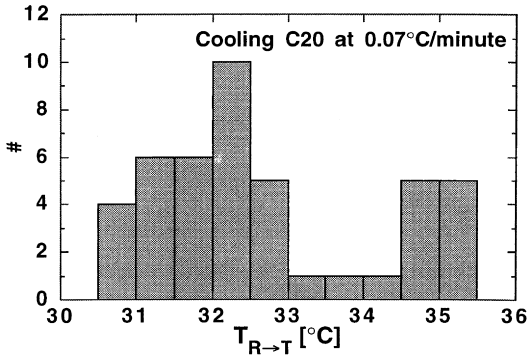

Fig. 13. A histogram of the observed temperatures of the R → T transition in C_{20} cooling at 0.07°C/min for multiple runs.

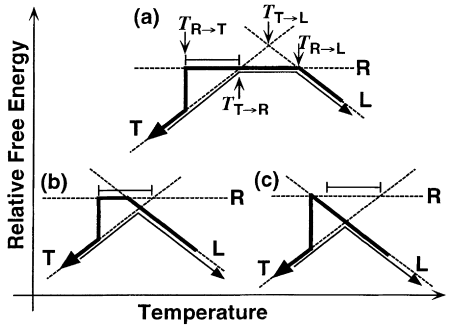

Fig. 14. Schematic showing the relative free energy (relative to the rotator phase) versus temperature for (a) a stable rotator phase (i.e. C_{24}), (b) a metastable rotator phase (C_{20}), and (c) a transient rotator phase (C_{16}). The dashed lines represent the equilibrium free energy curves for the three phases. The heavy and light solid line represents the path taken on cooling and heating, respectively. The bracket represents the difference between $T_{T\to R}$ and $T_{R\to T}$.

solutions and homogenous nucleation from the melt. (Homogeneous nucleation measurements, using the emulsion technique to eliminate heterogeneous nucleation effects from the bulk of the sample, yield supercoolings of 12–15°C.) If we were to suppose that homogeneous nucleation were limited by the energy barrier to nucleating into a transient rotator phase and relate the observed crystallization temperature to $T_{R\to L}$ rather than to $T_{T\to L}$, the even–odd variation observed in the homogeneous nucleation supercooling smoothes out [16–20]. This observation suggests that the low interfacial energies of the rotator phases may play a major role in crystal nucleation, not only with respect to the triclinic crystal phase of the *n*-even series, but also with respect to the orthorhombic crystal phases of the *n*-odd series, mixtures of both series, and solutions. Growth morphologies also depend on the crystal structure [46–48], and thus growth in a transient phase may impact morphology.

Recent studies of crystallization in both polymer [49–52] and other systems [53–55] suggest the existence of precursor phases with density higher than that of the liquid, but where the symmetry of the ordered phase is not fully developed. The rotator phases are similar in that their density is higher than the liquid and the symmetry is higher than the stable crystal (both quantities being intermediate).

Within the context of classical nucleation theory [17–19], nucleation will occur into a metastable phase if (using the spherical nucleus approximation) $\sigma_{ml}^3/[\Delta S_{ml}(T - T_{ml})]^2 < \sigma_{sl}^3/[\Delta S_{sl}(T - T_{sl})]^2$ at the crystallization temperature. Here σ are the surface energies, ΔS are the transition entropies, and s, m and l refer to stable, metastable and liquid. Transient phase induced nucleation may indeed be a very widespread effect since $\sigma_{ml} < \sigma_{sl}$ is a likely condition, especially for phases of intermediate order. Simulations, for instance, have shown rotator-like disorder at the solid–liquid interface of the orthorhombic crystal in alkanes [56]. Using the Gibbs–Thomson relation and the Hoffman–Weeks [57] expression for melting of laterally infinite, finite thickness lamellar crystals, Keller and collaborators [8–10] discussed at length the expected size dependence to the phase diagram. This implies a critical size above which a growing rotator-phase crystallite may convert to the stable orthorhombic structure.

Besides mediating crystallization on slow cooling, such transient phases may be frozen in by deep quenching. For example, the cycloparaffin nonadecylcyclohexane exhibits a rotator phase that is transient on slow cooling but remains indefinitely on deep quenching [58]. This result suggests that some phases that are reported to be formed only by deep quenching may indeed be transient states mediating crystallization at higher temperatures. This may be a mechanism at work in the formation of the quenched mesophase of isotactic polypropylene [43,59].

We have presented dramatic synchrotron X-ray evidence and a systematic chain-length study which finally explains the kinetics and supercooling in *n*-alkanes. We have detected a transient metastable rotator phase occurring on crystallization of hexadecane and octadecane into their triclinic phase from the supercooled melt. We then measured the crystallization kinetics of the homologous series of *n*-alkanes and explained it in terms of a crossover from stability to "long-lived" metastability to transient metastability.

We have directly shown that *n*-even alkanes without an equilibrium rotator phase crystallize via a metastable rotator phase. The relative stability of the rotator phase determines the observed crystallization temperature. This suggested that while the wax in dilute solutions precipitates in the equilibrium orthorhombic crystal phase, not the rotator phase; its precipitation is mediated and thus controlled by surface crystallization of a metastable rotator phase. This has been recently confirmed by adiabatic scanning calorimetry [60]. These results have strong implications for crystallization in polymer systems and are clear evidence of some the concepts which Keller had championed over the past decade.

Acknowledgements

We gratefully acknowledge discussions with Hubert King Jr., Moshe Deutsch, Henning Kraack, Ben Hsiao, Watson Srinivas and Jeff Hutter and the technical assistance of Steve Bennett and Wilton A. Gordon. The N.S.L.S. at B.N.L. is supported by the US Department of Energy, Divisions of Materials and Chemical Science.

References

[1] Keller A, Cheng SZD. Polymer 1998;39:4461.
[2] Ostwald W. Z Physik Chem 1897;22:286.
[3] Bassett DC, Turner B. Phil Mag 1974;29:925.
[4] Hikosaka M, Rastogi S, Keller A, Kawabata HJ. Macromol Sci B 1992;31:87.
[5] Hikosaka M, Amano K, Rastogi S, Keller A. Macromolecules 1997;30:2067.
[6] Keller A, Goldbeck-Wood G, Hikosaka M. Faraday Discuss 1993;95:109.
[7] Keller A. In: Dosiere M, editor. NATO ASI Series, vol 405. Dordrecht: Kluwer, 1993. p. 1.
[8] Keller A, Hilosaka M, Rastogi S, Toda A, Barham PJ, Goldbeck-Wood G. J Mater Sci 1994;29:2579.
[9] Keller A, Hikosaka M, Rastogi S, Toda A, Barham PJ, Goldbeck-Wood G. Phil Trans R Soc Lond A 1994;348:3.
[10] Keller A, Rastogi S, Hikosaka MH. Macromol Symp 1997;124:67.
[11] Keller A, Hikosaka M, Rastogi S. Physica Scripta 1966;T66:243.
[12] Rastogi S, Hikosaka M, Kawabata H, Keller A. Macromolecules 1991;24:6384.
[13] Small DM. The physical chemistry of lipids. New York: Plenum, 1986.
[14] Ungar G. Macromolecules 1986;19:1317.
[15] Sirota EB. Langmuir 1997;13:3849.
[16] Kraack H, Sirota EB, Deutsch M. J Chem Phys 2000;112:6873.
[17] Turnbull D, Cormia RL. J Chem Phys 1961;34:820.
[18] Uhlmann DR, Kritchevsky G, Straff R, Scherer G. J Chem Phys 1975;62:4896.
[19] Oliver MJ, Calvert PD. J Cryst Growth 1975;30:343.
[20] Herhold A, Ertas D, Levine AJ, King HE. Phys Rev E 1999;59:6946.
[21] Ross GS, Frolen LJ. J Res NBS A 1975;79:701.
[22] Cormia RL, Price FP, Turnbull D. J Chem Phys 1962;37:1333.
[23] Taggart AM, Voogt F, Clydesdale G, Roberts KJ. Langmuir 1996;12:5722.
[24] Sirota EB. Langmuir 1998;14:3133.
[25] Sirota EB, Herhold AB. Science 1999;283:529.
[26] Ewen B, Strobl GR, Richter D. Faraday Discuss Chem Soc 1980;69:19.
[27] Doucet J, Denicolo I, Craievich A. J Chem Phys 1981;75:1523.
[28] Denicolo I, Doucet J, Craievich AF. J Chem Phys 1983;78:1465.
[29] Ungar G. J Phys Chem 1983;87:689.
[30] Sirota EB, King Jr. HE, Singer DM, Shao HH. J Chem Phys 1993;98:5809.
[31] Sirota EB, King Jr. HE, Shao HH, Singer DM. J Phys Chem 1995;99:798.
[32] Sirota EB, King Jr. HE. Science 1998;281:143a.
[33] Sirota EB, Singer DM. J Chem Phys 1994;101:10 873.
[34] Weinstein A, Safran SA. Phys Rev E 1996;53:R45.
[35] Earnshaw JC, Hughes CJ. Phys Rev A 1992;46:4494.
[36] Wu XZ, Sirota EB, Sinha SK, Ocko BM, Deutsch M. Phys Rev Lett 1993;70:958.
[37] Wu XZ, Ocko BM, Sirota EB, Sinha SK, Deutsch M, Cao BH, Kim MW. Science 1993;261:1018.
[38] Ocko BM, Wu XZ, Sirota EB, Sinha SK, Gang O, Deutsch M. Phys Rev E 1997;55:3164.
[39] Gang H, Patel J, Wu XZ, Deutsch M, Gang O, Ocko BM, Sirota EB. Europhys Lett 1998;43:314.
[40] Wu XZ, Ocko BM, Tang H, Sirota EB, Sinha SK, Deutsch M. Phys Rev Lett 1995;75:1332.
[41] Sirota EB, Wu XZ, Ocko BM, Deutsch M. Phys Rev Lett 1997;79:531.
[42] Nyburg SC, Pickard FM, Norman N. Acta Cryst B 1976;32:2289.
[43] Wang ZG, Hsiao BS, Sirota EB, Agarwal P, Srinivas S. Macromolecules 2000.
[44] Nyburg SC, Lüth H. Acta Cryst B 1972;28:2992.
[45] Herhold AB, King HE, Sirota EB. Submitted for publication.
[46] Bennema P, Liu XY, Lewtas K, Tack RD, Rijpkema JJM, Roberts KJ. J Cryst Growth 1992;121:679.
[47] Liu XY, Bennema P. J Appl Cryst 1993;26:229.
[48] Liu XY, Bennema P. J Cryst Growth 1994;135:209.
[49] Imai M, Kaji K, Kanaya T, Sakai Y. Phys Rev B 1995;52:12 696.
[50] Ezquerra TA, Lopez-Cabarcos E, Hsiao BS, Balta-Calleja FJ. Phys Rev E 1996;54:989.
[51] Terrill NJ, Fairclough PA, Towns-Andrews E, Komanschek BU, Young RJ, Ryan AJ. Polym Commun 1998;39:2381.
[52] Olmsted PD, Poon WCK, McLeish TCB, Terrill NJ, Ryan AJ. Phys Rev Lett 1998;81:373.
[53] ten Wolde PR, Ruiz-Montero MJ, Frenkel D. Phys Rev Lett 1995;75:2714.
[54] Shen YC, Oxtoby DW. Phys Rev Lett 1996;77:3585.
[55] Schatzel K, Ackerson B. Phys Rev Lett 1992;68:337.
[56] Yamamoto TJ. Chem Soc Faraday Trans 1995;91:2559.
[57] Hoffman JD, Weeks JJ. J Chem Phys 1965;42:4301.
[58] Sirota EB, Herhold AB, Varma-Nair M. Submitted for publication.
[59] Brückner S, Meille SV, Petraccone V, Pirozzi B. Prog Polym Sci 1991;16:361.
[60] Sirota EB. J Chem Phys 2000;112:492.
[61] Broadhurst MG. J Chem Phys 1962;36:2578.